Structure, energetics, and molecular- to atomic-ordering transitions in hydrogen thin films

J. Z. Wu, S. B. Trickey, and J. R. Sabin
Quantum Theory Project, Department of Physics and Department of Chemistry, University of Florida, Gainesville, Florida 32611

J. C. Boettger
Theoretical Division, Los Alamos National Laboratory, Los Alamos, New Mexico 87545
(Received 8 August 1991)

One, two, and three layers of hydrogen display a rich variety of features, some intrinsic to ultrathin films, others essentially manifestations of crystalline H behavior. We present calculations, in the framework of local-density-functional theory, of the structure-energy behavior of 22 molecular and atomiclike H films in a variety of hexagonal, square, and rectangular symmetries. The equilibrium phases are molecular in character, subject to some modifications to account for the two-dimensional space group. Thus, the energetically flavored three-layer configuration (the low aspect ratio, $c/a<1$, hexagonal system) does not break up-down symmetry (one short and one long interlayer spacing, analogous with a possible linear H_3 geometry) because relaxation to this configuration is incompatible with the drastically different equilibrium intraplanar lattice spacings of the two possible component dilayers. Within the space groups and stackings considered, even the most energetically favored three-layer configuration (hexagonal with overhead stacking) is unbound with respect to the most-bound two-layer and one-layer configurations, an indication that layer-by-layer buildup of crystalline H will involve an intricate sequence of symmetries rather than simple epitaxy. The insulator-metal transition and two versions of the atomic-molecular ordering transition are investigated. For the monolayer transition from (molecular, square) to [monatomic, fcc (100)] ordering, the lattice constants change smoothly, whereas for the dilayer transition from molecularlike ($c/a<1$) to atomiclike ordering ($c/a>1$) the lattice constants change discontinuously.

I. INTRODUCTION

Zero-pressure solid hydrogen is a molecular crystal. As far back as 1935, Wigner and Huntington[1] proposed that instability at high pressures would lead to an atomic, metallic phase. As the lightest possible alkali metal, the large zero-point motion of crystalline atomic H suggests strong electron-phonon coupling, hence the possibility of high-T_c BCS superconductivity.[2] This occurrence of complex physical behavior in a system of very simple ingredients has made the sequence of crystalline phases of solid H a problem of continuing theoretical and computational interest. Monatomic structures (i.e., those in which the H atoms are translationally identical), molecular structures, and the associated ordering transitions in both crystals and one-dimensional (1D) chains have been treated.[3–14] Here we can summarize only the results most directly related to the present work.

Brovman, Kagan, and Kholas[3] systematically examined all possible lattices for the crystal structure of metallic hydrogen at $T=0$ K using a general many-body perturbation theory model. They found a trend toward less and less symmetric structure with decreasing pressure and predicted that the Bravais systems would exhibit triangular (i.e., hexagonal) in-plane order and multiple, nearly degenerate interplanar spacings separated by small energy barriers. In particular, they found that all the Bravais structures have energy minima both at $c/a<1$ (the so-called filamentary family) and $c/a>1$ (the so-called planar family), with a the intraplanar lattice constant and c the interplanar one. In every Bravais structure the filamentary case was predicted to be energetically favored. With increasing pressure, both minima shift toward the ideal value of c/a.

Wigner and Huntington[1] had conjectured the existence of metastable layered lattices intermediate in structural complexity and density between the high-pressure atomic phase and the $P=0$ molecular crystal. From their description it seems clear that these weakly bound layer structures are the planar structures of Ref. 3. Recently, Barbee *et al.*[7(a)] have predicted that a filamentary primitive-hexagonal phase with $c/a\approx 0.6$ is most stable in the intermediate-density regime, a finding in good agreement with the prediction of Ref. 3.

Chakravarty *et al.*[5] performed self-consistent calculations using density-functional theory in the local-density approximation (LDA). Their calculation used a spherical Wigner-Seitz cell for each molecule with the potential of the molecule initially averaged over rotations. Molecular symmetry was reintroduced perturbatively. Their most important prediction in the present context was that metallization is by band overlap in the molecular phase (prior to the transition to atomic ordering). Min, Jansen, and Freeman[6] have studied the structural properties and transitions of crystalline H using both the full-potential linearized augmented-plane-wave and linear-muffin-tin-

orbital methods to solve the LDA equations. They predict the simple cubic (sc) structure as the equilibrium paramagnetic atomic system,[6(a)] and pressure-induced metallization within the molecular phase at $P=1.7\pm0.2$ Mbar with the passage to the metallic atomic phase at 4 ± 1 Mbar[6(b)] (thus confirming Ref. 5).

There is also a lengthy tradition of investigating the molecular to atomic-ordering transition and related properties of solid H via calculations on periodically bounded linear chains.[8-14] In general, these calculations reproduce the properties of the crystal insofar as any crystal can have a faithful linear analog. Offhand, the same analogy might seem to hold for the relation of ultrathin layers of H to its crystalline phases. However, ultrathin systems with translational order in two dimensions and molecular-scale thickness in the third are known to have different properties from either their counterpart crystals or linear analogs.[15] It is immediately obvious that two kinds of molecular bonding are possible in ordered films. One, analogous to the molecular crystal, is the case in which not all atomic sites are equivalent by direct lattice translations. The other is the case in which an *interlayer* atomic distance is close to the H_2 bond length and notably smaller than the fundamental lattice translations.

For H these distinctions between crystals and free, ordered films raise questions as to how the molecular- to atomic-ordering transition will take place in an n-layer ($n=1,2,3$) configuration. Does filamentary structure dominate energetically even in an intrinsically layered system? Are the ordering transitions dominated by changes in interplanar or intraplanar bonding and are they strongly dependent on n or the 2D space group or both? Is there metallization in the molecularly ordered systems and, if so, how does it depend on n? Since the monatomic equilibrium phase is simple cubic while the H_3 linear molecule may have two drastically different bond lengths (the matter appears to be unresolved experimentally), does the H three-layer configuration (3L) exhibit a broken up-down symmetry? How similar are H and Li n-layer configurations, especially in the case of atomic ordering?

Except for our own preliminary report,[16] we are unaware of any previous work which deals with the detailed structure-energy relationships of H thin films. Here we consider both monatomic and molecular structures, the transition between them, and the onset of metallic behavior. For completeness, some results from Ref. 16 are included. In a subsequent paper[17] we shall present calculated proton stopping powers for these films.

II. METHODOLOGY AND SYSTEMS

Each system has two-dimensional translation symmetry (square, rectangular, hexagonal, graphitic) which is the same in all of its planes. The intraplanar lattice parameters are a and b, the interplanar lattice parameters are c_i ($i=1,2$) or simply c, as appropriate. Molecular bond lengths ("interproton" distances in some of the literature) are denoted by l_i. Hartree atomic units are used except where indicated (1 hartree = 27.2116 eV, 1 a.u.$=0.529\,177$ Å). The linear-combination-of-Gaussian-type-orbitals, fitting-function (LCGTO-FF) techniques[18] used to solve the Kohn-Sham (KS) equations (with Hedin-Lundqvist exchange-correlation potential) have been discussed elsewhere.[15] The method is all electron and full potential. All calculations reported here are paramagnetic. The current version of FILMS, the computer code embodying these techniques, differs primarily from previous versions in using improved numerical integral techniques.

The most important choices for a LCGTO-FF calculation are the three basis sets required. There is one for the KS orbitals, another for the charge density ("Q basis"), and a third for the LDA exchange-correlation kernels ("XC basis"). Several recent studies have shown the utility of using identical Q and XC bases, denoted hereafter as the F basis.

For the atomically ordered systems, the choices were identical $3s$-$1p$ KS and F sets, with s exponents of 0.151 398, 0.681 444, 4.5018, and a p exponent of 1.0. Some augmentation and refinement of the F basis was required as well. The s basis is from van Duijneveldt,[19] the p basis from previous experience.[18] Although it had not been customary to use identical KS and F bases, extensive testing on the square monolayer ($1L$) showed that doing so gave the best results (in the sense of least total energy and most accurate exchange-correlation fitting). Basis-set quality also may be judged from two other comparisons. First, for the square monatomic $1L$ at $a=2.65$ a.u., the total energy per atom from the $3s$-$1p$ basis and from a $6s$-$2p$ basis were $-0.533\,9585$ hartree/atom and $-0.537\,304\,1$ hartree/atom, respectively [using a Brillouin-zone (BZ) mesh of 21 points in the irreducible wedge]. Second, at $a=30.0$ a.u., the $3s$-$1p$ basis gives $-0.441\,887\,6$ hartree/atom, while an independent atomic calculation with a $10s$ basis and no fitting functions gives the isolated paramagnetic atomic energy as $-0.449\,034\,3$ hartree.

In the molecularly ordered systems, the F basis was augmented with an extra p-type function with exponent 0.8 aligned with the molecular axis at each nuclear site and contracted between sites with opposite sign. The numerical shift from this augmentation is illustrated by the case of a square molecular $1L$ with the molecular axis aligned along the square diagonal. When the molecular bond length is half the diagonal [fcc(100)], the difference due to augmentation (which should be zero) is less than 0.001 mhartree. At more realistic molecular bond lengths, the improvement from augmentation is more than three orders of magnitude larger. For those $3L$'s with up-down symmetry, the p-type fitting functions associated with the two outer layers were contracted into symmetric and antisymmetric pairs. In the $c_1>c_2$ cases, bond-centered s-type-fitting-basis functions with exponents 1.000 and 0.800 (for the c_1 and c_2 midpoint sites, respectively) were used as well.

In the special case of dense square $1L$'s, approximate linear dependencies intrude for atomic areal densities greater than about 0.208 atom/a.u.^{2}. Therefore, above 0.208 atom/a.u.^{2}, in the square $1L$ only, the exponents of both the KS and F bases were increased by 0.0065. Table I shows this and similar additional basis-set consolidation

TABLE I. Incremental shifts in basis-set exponents as a function of areal density in the square $1L$ (only). The shifts are *not* cumulative.

Areal density (atom/bohr^2)	Exponent increment (bohr^{-2})
0.2081	0.0065
0.0222	0.0172
0.2378	0.0320
0.2551	0.0420
0.2664	0.0500
0.2743	0.0570
0.2958	0.0740

required with increasing areal density. There is no evidence that the consolidation introduced any significant biases or discontinuities in calculated system properties as functions of lattice spacings.

All together, 22 kinds of films (i.e., combinations of layer number and symmetry) were treated. The labeling convention adopted is as follows: M denotes monolayer, D denotes dilayer, T denotes trilayer, a denotes atomic, m denotes molecular, R denotes rectangular, S denotes square, H denotes hexagonal, G denotes graphitic, Op denotes open, Ov denotes overhead, and E denotes eclipsed. Subscripts ">" and "<" indicate $c > a$ or $c < a$, respectively. Thus $D_>$ (S,Op) denotes a two-layer structure ($2L$) with $c > a$, square symmetry, and open re-

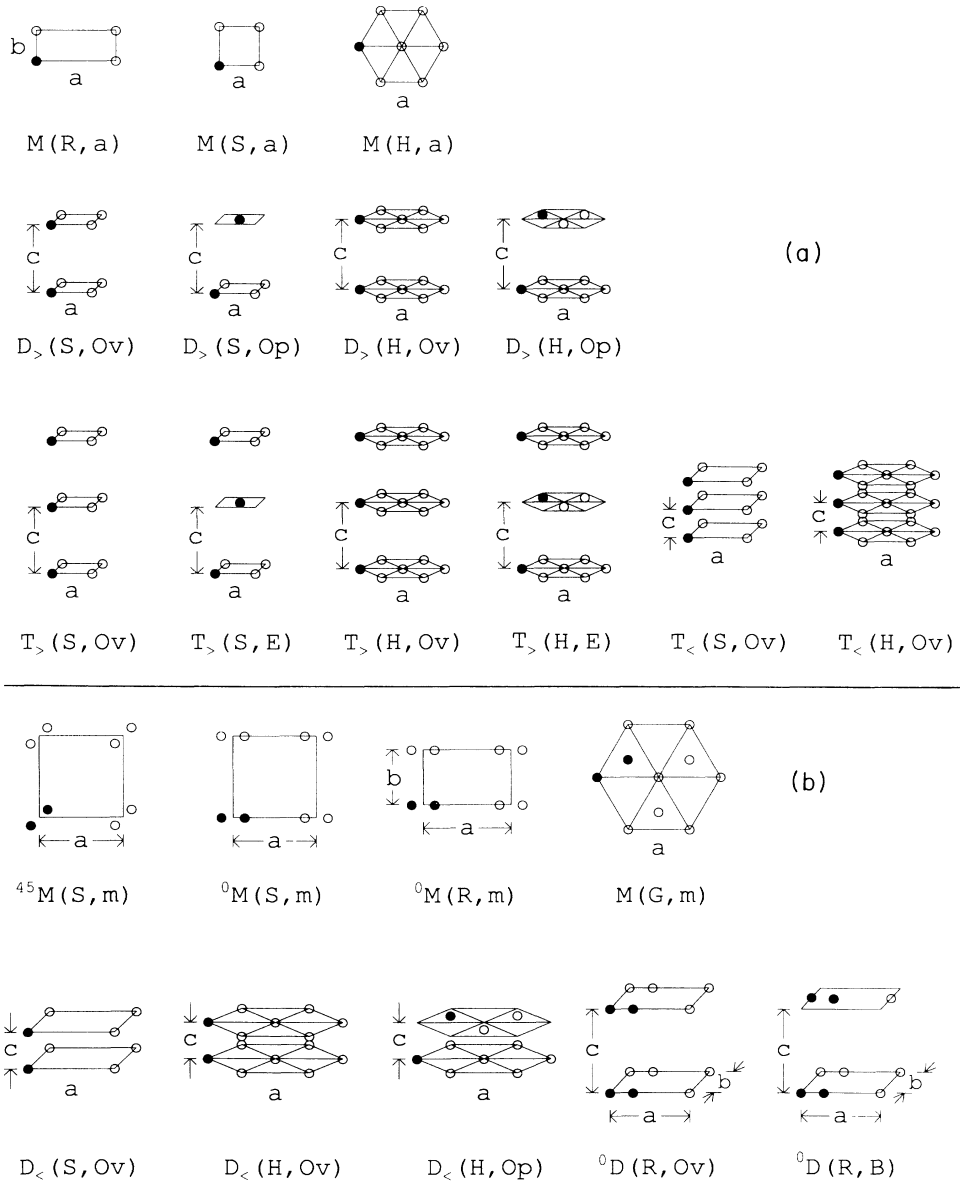

FIG. 1. Diagrammatic representation of the systems treated. Solid dots represent the atoms in a single unit cell. (a) Monatomic structures; (b) molecular structures. Note that $D_<$(H,Op) at $c = 0$ (which turns out to be the energetically preferred value) is the same as M(G,m).

gistry of the two nuclear planes. The list is as follows.

(1) $1L$, rectangular; atomic, $M(R,a)$; (2) $1L$, square; atomic, $M(S,a)$; (3) $1L$, hexagonal; atomic, $M(H,a)$; (4) $1L$, hexagonal graphitic; molecular [the planar limit of $D_<(H,\mathrm{Op})$], $M(G,m)$; (5) $1L$, rectangular; molecular, with the molecule centered at the lattice site and aligned along the a axis, ${}^0M(R,m)$; (6) $1L$, square; molecular, (a) the molecule is centered at the lattice site and is aligned along the a axis, ${}^0M(S,m)$; (b) the molecule is centered at the lattice site and is aligned along the square diagonal, ${}^{45}M(S,m)$; (7) $2L$ and $3L$, square 2D Bravais lattice; overhead orientation of the two or three planes, specified c/a: $D_<(S,\mathrm{Ov})$, $T_<(S,\mathrm{Ov})$, $D_>(S,\mathrm{Ov})$, $T_>(S,\mathrm{Ov})$; (8) $2L$ and $3L$, square 2D Bravais lattice; open orientation of the two planes (i.e., the atomic nuclei in one layer reside directly above the square center in the other layer) and eclipsed orientation of three planes (i.e., the atomic nuclei in the first and third layers reside directly above and below the square center in the midlayer), $c/a>1$: $D_>(S,\mathrm{Op})$, $T_>(S,E)$; (9) $2L$ and $3L$, hexagonal 2D Bravais lattice; overhead orientation of the two or three planes, specified c/a: $D_<(H,\mathrm{Ov})$, $T_<(H,\mathrm{Ov})$, $D_>(H,\mathrm{Ov})$, $T_>(H,\mathrm{Ov})$; (10) $2L$ and $3L$, hexagonal 2D Bravais lattice; open orientation for the $2L$ and eclipsed orientation for the $3L$, specified c/a: $D_<(H,\mathrm{Op})$, $D_>(H,\mathrm{Op})$, $T_>(H,E)$; (11) $2L$, rectangular 2D Bravais lattice; overhead orientation, essentially a $2L$ of two ${}^0M(R,m)$'s: ${}^0D(R,\mathrm{Ov})$; (12) $2L$, rectangular 2D Bravais lattice; bridge orientation with respect to one Bravais axis, a different way to make a $2L$ from two ${}^0M(R,m)$'s: ${}^0D(R,B)$. Note that we are compelled to classify the monolayer graphitic structure as molecular, although the bond length is much longer than in any of the other molecular systems.

The systems are diagramed in Figs. 1(a) (atomic systems) and 1(b) (molecular systems). (It turns out that $c_1=c_2$ for the energetic minima of the $3L$'s; see below.) We have investigated two kinds of structural phase transition. In the $2L$ systems this was from $c<a$ to $c>a$. In the $1L$ the transition is from the 45° molecular orientation to the fcc(100) monatomic structure.

The simple observation that fcc(100) with edge length a is the same as a simple square (100) with edge length $a/\sqrt{2}$ suggests the importance of the corresponding relationship among various Brillouin-zone irreducible segments associated with the differing systems. At issue is the extreme sensitivity of calculated total energies and optimized lattice parameters to the number of BZ points, a problem already emphasized in solid H by Min, Jansen, and Freeman.[6(a)] The diversity of n layers all requiring the same precision makes the problem at least as acute for this work. [Irreducible regions for all cases except ${}^{45}M(S,m)$ are given explicitly by Terzibaschian and Enderlein.[20]]

Figure 2 illustrates the issue. It shows the lattice structure, the irreducible BZ wedge, and the two rather natural BZ choices for the ${}^{45}M(S,m)$ configuration in the special case $l=a/\sqrt{2}$ with a the fcc(100) lattice parameter. The smaller BZ corresponds to primitive translations $\mathbf{R}_1=a(1,0)$, $\mathbf{R}_2=a(0,1)$ and two atoms per cell at either the conventional fcc sites [$a(0,0)$ and $a(\frac{1}{2},\frac{1}{2})$] or at the equivalent but more molecular-appearing $a(\frac{1}{4},\frac{1}{4})$ and $-a(\frac{1}{4},\frac{1}{4})$; only the latter choice is illustrated. That smaller BZ is the square bounded by a solid line in Fig. 2(b) and the corresponding irreducible region is one-half of the cross-hatched BZ quadrant. The dashed square shows the other natural BZ boundary for the fcc(100) configuration, namely for one atom per unit cell on the simple square lattice [primitive translations $\mathbf{R}_1'=(a/2)(1,1)$, $\mathbf{R}_2'=(a/2)(-1,1)$]. Clearly, some quite different BZ scans and precisions can occur for systems that are, in fact, identical unless due care is taken.

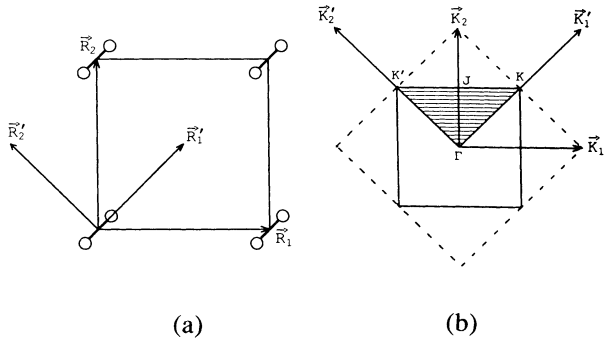

FIG. 2. (a) Lattice-structure and (b) associated BZ choices for the ${}^{45}M(S,m)$ configuration. The solid square is the BZ boundary for the ${}^{45}M(S,m)$ lattice and two atoms per cell; the dashed square is the corresponding BZ for the fcc(100) treated as one atom per cell. The shaded irreducible wedge and associated labeled symmetry points are for the smaller BZ.

Figures 3(a)–3(d) show the sensitivity of various calculated quantities to BZ mesh density as measured by the number of triangles in the irreducible BZ (FILMS uses the linear triangle analog of the linear analytical tetrahedron method). Figures 3(a) and 3(b) show the mesh-density dependence of the optimized lattice constant and the Fermi energy ε_F for $M(S,a)$. Both stabilize smoothly, but at a relatively high number of points in the BZ.

Figure 3(c) shows the dependence of E_{tot}/N on mesh density for four different l,a pairs in the ${}^{45}M(S,m)$ system. The two more extensive curves (long-dashed and solid) are for the special case $l=a/\sqrt{2}$ with a the fcc(100) lattice parameter. From these one sees that E_{tot}/N stabilizes at a lower BZ mesh density for the energetically favored case ($a=4.38$ a.u., the long-dashed curve) than for the unfavored, compressed case ($a=2.8$ a.u., the solid curve). When l is energy optimized the trend is even stronger [note that the dotted curve in Fig. 3(c) is shifted *upward* by 0.04 hartree/atom in order to get it into the same figure]. In both cases the increased $|\nabla_{\mathbf{k}}\varepsilon_{j\mathbf{k}}|$ that accompanies compression is the source of the increased sensitivity to mesh density.

Figure 3(d) shows the dependence of the calculated minimum-energy molecular bond length for fixed $a=2.8$ a.u. in ${}^{45}M(S,m)$. Evidently, one of the most demanding tasks is to determine the molecular bond length corresponding to a specified a, especially at high atomic areal densities.

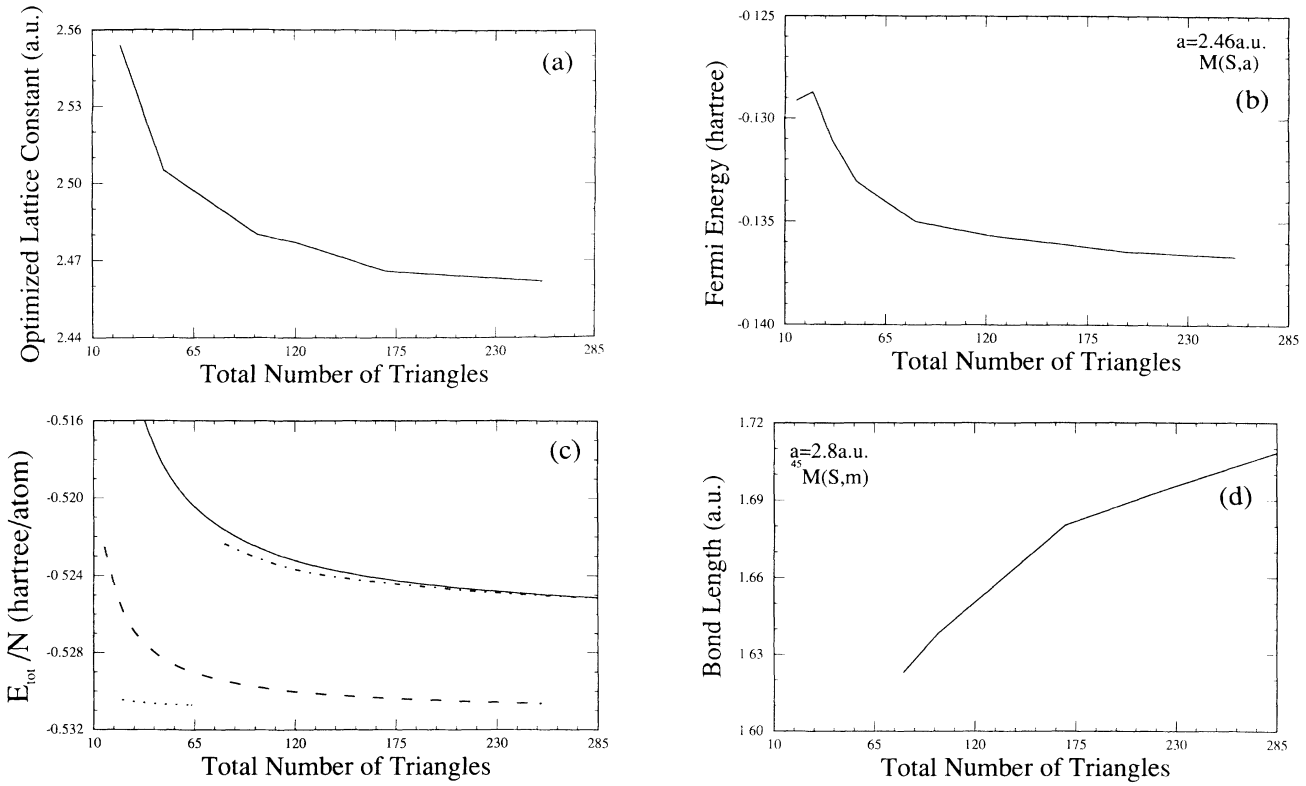

FIG. 3. Sensitivity of calculated quantities to BZ mesh density. (a) Optimized lattice constant of the $M(S,a)$ system; (b) Fermi energy ε_F for $M(S,a)$ at $a=2.46$ a.u., the calculated equilibrium value; (c) total energy per atom $E_{\rm tot}/N$ for $^{45}M(S,m)$: long-dashed curve is $a=4.38$ a.u. with $l=a/\sqrt{2}$, solid curve is for the same special case but with $a=2.8$ a.u., dotted curve (*raised* by 0.04 hartree/atom) is for $a=5.7$ a.u. and the energy-optimized l, dash-dotted curve is for $a=2.8$ a.u. and the energy-optimized l; (d) minimum-energy molecular bond length for $^{45}M(S,m)$ with fixed $a=2.8$ a.u. The kink at 1.68 a.u. is due to the discontinuity of polynomial fitting points chosen.

The calculations reported used up through 361 triangles in the irreducible quarter of the BZ for $M(S,a)$ at an areal density of 0.295 atom/a.u.^{2} and 324 triangles for $^{45}M(S,m)$ at an areal density of 0.274 atom/a.u.^{2}. We estimate the imprecision of total energies due to the BZ mesh as ± 0.5 mhartree. The corresponding uncertainty in the optimized lattice parameters is ± 0.02 a.u. The mesh-induced error in the calculated molecular bond length tends to be larger, especially in a region near the transition from molecular to atomic behavior, where it may be as much as ± 0.05 a.u. Optimized lattice constants and bond lengths were determined by a quadratic fit to the nearest three points since, for some cases, the energy valleys are narrow and shallow, thus requiring that the fitting points be chosen quite close to the energy minimum.

III. RESULTS

A. Optimized structures at zero stress

The calculated equilibrium lattice constants and total energies per atom for all the atomic and molecular H nL's are shown in Table II. First among the striking features is that the most-bound $2L$'s $^0D(R,B)$ and $^0D(R,\mathrm{Ov})$ are barely bound (within calculational precision) with respect to two molecularly ordered $1L$'s. None of the high-symmetry $3L$'s treated here is bound with respect to separation to three of the molecularly ordered $1L$'s, nor are they bound with respect to the combination of either of the two most-bound high-symmetry $2L$'s, $D_<(H,\mathrm{Ov})$ and $D_<(S,\mathrm{Ov})$, plus one of the (nearly degenerate) energetically favored $1L$'s.

Clearly, the in-plane H_2 chains characteristic of all the molecular $1L$'s and of the energetically preferred $2L$'s are favored in comparison with even a dimerized $2L$, whose molecules are aligned perpendicular to the translational symmetry plane. Everything we have seen argues for the dominance of filamentary structures at all levels of aggregation. The calculations thus suggest that formation of crystalline H is not by simple atomic epitaxial growth on either a hexagonal or square 2D atomiclike lattice. While for technical reasons none of the $2L$ or $3L$ structures considered here is a slice from the $Pa3$ crystal (the known ground state for crystalline ortho-H_2), our results are also consistent with the general finding that molecular ordering is always preferred in cases of zero stress.

Table II also shows two notable $2L$ features. For a given stacking (open or overhead) and c/a class (filamentary, planar), the higher symmetry $2L$'s are energetically

TABLE II. Calculated equilibrium total energies per atom (E_{tot}/N; hartree per atom) and lattice parameters (a.u.) for H nL's, ordered from the most to the least bound within each family. The intraplanar lattice parameters are a and b, l is the H_2 bond length, s is the intermolecular spacing (end to end) along the molecular axis, and c is the interplanar spacing. Note that l was optimized for the rectangular $1L$'s, then that value was held fixed for the rectangular $2L$'s. $M(G,m)$ and $D_<(H,\mathrm{Op})$ are marked with an asterisk because, while they are conceptually different, they turn out to be degenerate. See text for structure labeling.

System	a	b	c	c/a	l	s	$-E_{tot}/N$
${}^0M(R,m)$	5.05	5.47			1.45	3.60	0.5713
${}^0M(S,m)$	5.33	5.33			1.46	3.87	0.5711
${}^{45}M(S,m)$	5.62	5.62			1.45	6.50	0.5706
$M(R,a)$	4.84	1.91					0.5582
$M(G,m)^*$	3.88				2.24	4.48	0.5549
$M(H,a)$	2.61						0.5434
$M(S,a)$	2.46	2.46					0.5428
${}^0D(R,B)$	5.06	5.53	4.89	0.97	1.45	3.60	0.5716
${}^0D(R,\mathrm{Ov})$	5.06	5.49	5.43	1.07	1.45	3.61	0.5715
$D_<(H,\mathrm{Ov})$	5.44		1.46	0.27	1.46		0.5697
$D_<(S,\mathrm{Ov})$	5.39	5.39	1.46	0.27	1.46		0.5695
$D_<(H,\mathrm{Op})^*$	3.88		0.00	0.00	2.24	4.48	0.5549
$D_>(H,\mathrm{Ov})$	2.62		4.37	1.67			0.5443
$D_>(H,\mathrm{Op})$	2.62		4.37	1.67			0.5443
$D_>(S,\mathrm{Ov})$	2.48	2.48	4.23	1.71			0.5437
$D_>(S,\mathrm{Op})$	2.47	2.47	4.32	1.75			0.5437
$T_<(H,\mathrm{Ov})$	3.80		1.78	0.47			0.5527
$T_<(S,\mathrm{Ov})$	3.70	3.70	1.77	0.48			0.5514
$T_>(H,\mathrm{Ov})$	2.62		4.22	1.61			0.5448
$T_>(H,E)$	2.62		4.15	1.58			0.5447
$T_>(S,\mathrm{Ov})$	2.47	2.47	4.06	1.64			0.5442
$T_>(S,E)$	2.47	2.47	4.11	1.66			0.5441

indifferent to the translational symmetry, square or hexagonal. Furthermore the $2L$'s with $c>a$ and fixed translational symmetry are energetically insensitive to the stacking choice. Both features are signatures of the dominance of molecular character in the structural energetics.

1. Monolayers

Among the atomic $1L$'s, $M(R,a)$ is analogous to a structure of linear chains with intrachain spacing b and interchain spacing a. Since interchain binding is weaker than intrachain binding, its total energy is less sensitive to changes of the interchain spacing than of intrachain spacing. The $M(R,a)$ structure is also geometrically equivalent to a planar slice from an ordered linear-chain bundle in bulk, with the slice parallel to the chain direction and interchain spacing a. Hence $M(R,a)$ is a monatomic $1L$ analog of the filamentary structures studied by Brovman, Kagan, and Kholas.[3]

The fact that the atomic $1L$'s are energetically ordered as $E_{M(R,a)}<E_{M(H,a)}<E_{M(S,a)}$, i.e., a preference for one bond substantially shorter than the other, already signals the favored nature of a filamentary ordered structure. The molecular $1L$'s order as $E_{0_{M(R,m)}}\sim E_{0_{M(S,m)}}<E_{45_{M(S,m)}}<E_{M(G,m)}$. The penultimate difference in energies is within the limits of numerical precision, so that the genuinely molecularly ordered $1L$'s are predicted to be nearly degenerate. [$M(G,m)$ is an oddity from the perspective of classification, an anomaly already mentioned.]

More importantly, $E_{M(X,m)}<E_{M(Y,a)}$ for all choices of X, Y, rectangular, hexagonal, and square. Even at the $1L$ level, the predominance of molecular bonding is quite evident. This predominance also shows up in the optimized molecular bond length in all three genuinely molecular $1L$'s. It is quite close to the experimental value for the free H_2 molecule (1.401 a.u.).[21] An interesting feature of the molecular $1L$'s is the suggestion of energetic advantage for lowered symmetry, namely rectangular as opposed to square. Numerical precision limits the interpretation.

2. Dilayers

Table II shows several notable $2L$ features. For a given stacking (open or overhead) and c/a class (filamentary, planar), the higher-symmetry $2L$'s are energetically indifferent to the translational symmetry, square or hexagonal. As noted at the outset of this section, the planar $2L$'s are so dominated by molecular ordering that for a given translational symmetry they are energetically insensitive to the stacking choice. This is particularly striking in the two rectangular systems, which are essentially a pair of slightly relaxed minimum-energy $1L$'s.

The $2L$'s are energetically ordered as

$E_{^0D(R,B)} \sim E_{^0D(R,\mathrm{Ov})} < E_{D_<(H,\mathrm{Ov})} \sim E_{D_<(S,\mathrm{Ov})} < E_{D_>(H,\mathrm{Ov})} = E_{D_>(H,\mathrm{Op})} < E_{D_>(S,\mathrm{Ov})} = E_{D_>(S,\mathrm{Op})}$. Intraplanar dimerization is built into the first two, while interplanar dimerization is unmistakable for the next pair. Thus, c for $D_<(H,\mathrm{Ov})$ and $D_<(S,\mathrm{Ov})$ are essentially identical with l for $^{45}M(S,m)$: $c_{D_<(H,\mathrm{Ov})} \sim c_{D_<(S,\mathrm{Ov})} \sim l_{^{45}M(S,m)} = 1.46$ a.u. All are rather close to the H_2 molecular bond length of 1.401 a.u. (Ref. 21). Another indicator of dimerization is that the total energies per atom of $^0D(R,B)$, $^0D(R,\mathrm{Ov})$, $D_<(S,\mathrm{Ov})$, $D_<(H,\mathrm{Ov})$, $^{45}M(S,m)$, $^0M(S,m)$, and $^0M(R,m)$ differ over a range of only 2 mhartree while they differ from the systems with atomic (layered) ordering by 20–28 mhartree.

Both filamentary hexagonal systems $D_<(H,\mathrm{Ov})$ and $D_<(S,\mathrm{Ov})$ are well bound with respect to a hexagonal $1L$ but unbound with respect to the minimum-energy $1L$, $^0M(R,m)$. As noted, $D_<(H,\mathrm{Op})$ is an interesting case in that its energy minimum occurs at the graphitic $1L$, i.e., $c=0$. Among the $2L$'s, both the $D_<(S,\mathrm{Ov})$ and $D_<(H,\mathrm{Ov})$ structures have geometries corresponding to slices perpendicular to the molecular chain for certain of the predicted high-pressure phases of crystalline H_2.[7(a)] $D_<(S,\mathrm{Ov})$ and $D_>(S,\mathrm{Ov})$ are distinguished as are the pair $D_<(H,\mathrm{Ov})$ and $D_>(H,\mathrm{Ov})$ because of the observations made by Brovman, Kagan, and Kholas[3] regarding nearly degenerate structures with c/a values both >1 and <1.

To treat the interplanar binding energy for an nL usefully one must distinguish delamination into equilibrium $1L$'s from delamination into $1L$'s constrained to have the same $2D$ space group as the nL. The equilibrium value per atom is defined as $\Delta_0 = E_{\mathrm{tot}}^{nL,0}/N - E_{\mathrm{tot}}^{1L,0}/N$, where the index zero indicates the lowest-energy configuration for the $1L$ and nL, irrespective of any symmetry change between the two. The symmetry-constrained counterpart is $\Delta_{C,i} = E_{\mathrm{tot}}^{nL,i}/N - E_{\mathrm{tot}}^{1L,i}/N$ with i indicating R, H, or S, as appropriate.

Table III shows that none of the $2L$'s is even marginally stable against a symmetry-changing delamination into a pair of $^0M(s,m)$ $1L$'s. That is, even $\Delta_0 = -0.3$ mhartree for $^0D(R,B)$ is smaller in magnitude than the estimated precision, 1 mhartree, of a total-energy difference. As measured by either Δ_0 or $\Delta_{C,i}$, the undimerized high-symmetry (hexagonal and square) dilayers are far less stable against delamination than the two dimerized systems [$D_<(S,\mathrm{Ov})$ and $D_<(H,\mathrm{Ov})$], a striking illustration of the energy advantage of dimerization. In both measures, more than an order of magnitude in delamination energy is gained via dimerization. As evident from the almost vanishing symmetry-constrained interplanar binding energy ($\Delta_{C,i} = -0.001$ hartree/atom) and the a lattice parameters, the high-symmetry $2L$'s with $c/a > 1$ behave essentially as two weakly attracting atomiclike $1L$'s.

3. Trilayers

From the $1L$ and $2L$ results it is clear that the obvious candidate for the energetically favored $3L$ is a stack of rectangular, molecular, filamentary $1L$'s. Two technical aspects combine with a conceptual problem to make treating that system less interesting than at first might be thought. The technical aspects are that the system has six atoms per unit cell and five lattice parameters to optimize (a, b, c_1, c_2, and l), hence the calculation would be laborious at best. The conceptual problem is that the very obviousness of these parallel slices from the filamentary solid means that they are of limited interest since there can be little doubt from the $1L$, $2L$, or crystalline results what the outcome would be; a laborious sequence of calculations merely to confirm that appraisal had limited appeal.

In contrast, the behavior of films whose structure is sliced perpendicular to the filamentary axis is harder to intuit. For example, at $3L$'s a new lattice parameter possibility occurs, namely the breaking of up-down symmetry, $c_1 \neq c_2$. The possibility is addressed most straightforwardly by restricting consideration to the overhead alignment. Calculations on gas-phase linear H_3 show no evidence[22] for equilibrium bond-length asymmetry, although nonequilibrium asymmetric structures lie lower on the calculated-potential surface than symmetric ones (the potential surface is repulsive).

Similarly, we find no evidence for a broken up-down symmetry in the overhead H $3L$'s. A thought experiment

TABLE III. Calculated constrained and equilibrium interplanar binding energies ($\Delta_{C,i}$, Δ_0; hartrees per atom) for hydrogen $2L$'s in eight structures at the calculated equilibrium lattice constants a, b, c. For $^0D(R,B)$ and $^0D(R,\mathrm{Ov})$ the values shown are as calculated but are smaller in magnitude than the estimated precision in a total-energy difference, 0.001 hartree. The systems are ordered from the most to the least bound.

System	a	b	c	c/a	$\Delta_{C,i}$	Δ_0
$^0D(R,B)$	5.06	5.53	4.89	0.97	−0.0003	−0.0003
$^0D(R,\mathrm{Ov})$	5.06	5.49	5.43	1.07	−0.0002	−0.0002
$D_<(H,\mathrm{Ov})$	5.44		1.46	0.27	−0.026	+0.002
$D_<(S,\mathrm{Ov})$	5.39		1.46	0.27	−0.027	+0.002
$D_>(H,\mathrm{Ov})$	2.62		4.37	1.67	−0.001	+0.027
$D_>(H,\mathrm{Op})$	2.62		4.37	1.67	−0.001	+0.027
$D_>(S,\mathrm{Ov})$	2.48		4.23	1.71	−0.001	+0.028
$D_>(S,\mathrm{Op})$	2.47		4.32	1.75	−0.001	+0.028

on the two possible component $2L$'s using the calculated results for the square $2L$'s illustrates why this happens in the square $3L$ with unequal c_i's. Denote the supposedly shorter H_3 bond length as l_1. If one sets it to the free H_2 bond length, then the proper component $2L$ with which to make identification is $D_<(S,\mathrm{Ov})$ ($c=1.46$ a.u. versus $l_1=1.41$ a.u.), hence a is set at about 5.4 a.u. Alternatively, one can go out the H_3 potential surface to a low-energy (nonequilibrium) molecular configuration that is asymmetric and still has $l_1=1.41$ a.u. (Ref. 22). Such configurations typically have $l_2=4.3$ a.u. or so. This suggests that the relevant $2L$ for identification with is $D_>(S,\mathrm{Ov})$ (from Table II: $c=4.23$ a.u.), whence the component intraplanar lattice parameter is about $a=2.5$ a.u. The evident point is that the attempt to keep at least one of the H_3 bonds close to the H_2 value while breaking up-down symmetry will introduce large in-plane strains. In fact, the unequal bond system relaxes those strains to an a value not far from the average of the two $2L$'s (3.84 a.u. actual versus 3.95 average).

For the equilibrium $3L$'s (equal c_i's) the energetic ordering is $E_{T_<(H,\mathrm{Ov})}<E_{T_<(S,\mathrm{Ov})}<E_{T_>(H,\mathrm{Ov})}\sim E_{T_>(H,E)}<E_{T_>(S,\mathrm{Ov})}\sim E_{T_>(S,E)}$. In view of the $2L$ results, the relationships among the $3L$'s exhibit no qualitative surprises: $c/a<1$ is favored because it can give a somewhat molecular $c=1.77$ a.u. while hexagonal structure is energetically favored because of packing.

Considered among themselves, the energetic ordering of the $3L$'s matches the predictions of Brovman, Kagan, and Kholas[3] for the crystal. The quasifilamentary structures, i.e., those with $c/a<1$[$T_<(S,\mathrm{Ov})$ and $T_<(H,\mathrm{Ov})$], should be energetically favored as compared with the planar ones [$T_>(S,\mathrm{Ov})$, $T_>(S,E)$, $T_>(H,\mathrm{Ov})$, and $T_>(H,E)$]. Because these are, from the crystalline perspective, slices perpendicular to the filamentary axis, this class of filamentary $3L$'s is energetically disadvantaged with respect to both long-chain filamentary $3L$'s and filamentary $1L$ and $2L$'s. The energetic preference for hexagonal ordering over square ($E_{T_<(H,\mathrm{Ov})}<E_{T_<(S,\mathrm{Ov})}$) for the quasifilamentary structure also matches the prediction of Ref. 3 that what they denote as the triangular filamentary family is energetically favored over the quadratic filamentary family.

The near equalities $E_{T_>(H,\mathrm{Ov})}\sim E_{T_>(H,E)}$, $E_{T_>(S,\mathrm{Ov})}\sim E_{T_>(S,E)}$ and the very large c/a in both cases are at least consistent with the interpretation that the interplanar binding in these cases is largely van der Waals in character. The energy barrier between the two stackings (overhead, eclipsed) is not readily calculable because of numerical difficulties in maintaining uniform precision limits while passing from one rather high-symmetry structure to another through a series of lower-symmetry ones. Nevertheless, the degeneracy found in both hexagonal and square symmetries may indicate a rather soft shear modulus for sliding the planes over one another.

It was remarked earlier that the crystalline calculations of Barbee *et al.*[7(a)] find that for $P>380\pm50$ GPa, the primitive-hexagonal phase with $c/a\approx0.6$ is most stable. Although the $T_<(S,\mathrm{Ov})$ structure has an even more dramatically anisotropic c/a, our finding is consistent with Barbee *et al.*, particularly when the possibility of bond contraction owing to a vacuum exterior (as opposed to a crystalline one) is taken into account.

4. *Layer-number dependencies*

The behavior of structural energetics as a function of n can be appraised in a variety of ways. We focus first on fixed stacking, then on minimum-energy configurations. Table IV gives the n dependence of the overhead stacked systems.

For both square and hexagonal films a general trend is evident in the case of $c>a$: c decreases modestly, a is stable, and the systems become slightly more bound with increasing n. Further, E_{tot}/N is almost independent of stacking or number of layers. All of these features are consistent with the description of the $c>a$ n layers as extremely weakly bound assemblies of $1L$'s.

No such trend is evident for square and hexagonal systems with $c<a$, a manifestation of the fact that all the

TABLE IV. Comparison of energy and structure n dependencies ($n=1,2,3$) for the square and hexagonal overhead cases. Note that $M(H,a)$ is included twice and that ${}^0D(R,\mathrm{Ov})$ is included for convenience of comparison, E_{tot}/N is the total energy per atom; a, b, c are the equilibrium lattice parameters.

System	a	b	c	c/a	$-E_{\mathrm{tot}}/N$
$M(H,a)$	2.61				0.5434
$D_>(H,\mathrm{Ov})$	2.62		4.37	1.67	0.5443
$T_>(H,\mathrm{Ov})$	2.62		4.22	1.61	0.5448
$M(S,a)$	2.46	2.46			0.5428
$D_>(S,\mathrm{Ov})$	2.48	2.48	4.23	1.71	0.5437
$T_>(S,\mathrm{Ov})$	2.47	2.47	4.06	1.64	0.5442
$M(H,a)$	2.61				0.5434
$D_<(H,\mathrm{Ov})$	5.44		1.46	0.27	0.5697
$T_<(H,\mathrm{Ov})$	3.80		1.78	0.47	0.5527
$M(R,a)$	4.84	1.91		0.39 (b/a)	0.5582
$D_<(S,\mathrm{Ov})$	5.39	5.39	1.46	0.27	0.5695
$T_<(S,\mathrm{Ov})$	3.70	3.70	1.77	0.48	0.5514
${}^0D(R,\mathrm{Ov})$	5.06	5.49	5.43	1.07	0.5715

$2L$'s are closely related to the H_2 molecule, whereas the $3L$'s are less well related to the H_3 molecule. While all the $c<a$ cases are n-layer filamentary structures in the literal sense of the definition of Brovman *et al.*,[3] the fact that they are slices across filaments in the corresponding crystal means that any residual chains are in-plane, orthogonal to their crystalline counterparts. Reflection on Table IV will confirm that the result is a set of intrachain separations and interchain distances which is dominated by the opportunities for dimerization in the various systems, not the ancestral crystalline filamentary structure. Thus the filamentary $2L$'s [$D_<(S,\mathrm{Ov})$, $D_<(H,\mathrm{Ov})$] have interchain spacing of $c=1.46$ a.u. but intrachain spacing of 5.39 a.u., while the same quantities for the $3L$ analogs are 1.77 and 3.7–3.8 a.u., respectively. For the rectangular $1L$ $M(R,a)$, the intrachain spacing, 1.91 a.u., is reassuringly close to the 1.88 a.u. calculated for linear chains[11] and rings.[9,10]

B. Structural transitions

Brovman, Kagan, and Kholas[3] predicted that in crystalline H, "all the uniaxial structures have energy minima both at $c/a<1$ and at $c/a>1$, but the latter lie higher in energy at $P=0$. With increasing pressure, both minima shift towards the ideal value c/a." The $2L$ which is analogous in the sense of corresponding to a 3D Bravais lattice is $D(S,\mathrm{Ov})$. Figure 4 shows the total energy per atom and optimized interplanar distance c, as functions of the lattice parameter a for both the molecular ($c<a$) and monatomic ($c>a$) versions of this $2L$. (For the molecular $2L$, points below $a=2.7$ a.u. are not shown because the energy valley is too flat as a function of c to allow reliable determination of the minimum.) Clearly, c for the molecular $2L$ at its own equilibrium is very close to the isolated molecule bond length of 1.401 a.u.

The prediction of Brovman, Kagan, and Kholas is equivalent to two implicit claims. In the case of $D_<(S,\mathrm{Ov})$, the first is that the energies of the $c<a$ and $c>a$ structures merge smoothly as a function of a. Figure 4 shows clearly that such is not the case. The second implicit claim is that the appropriate way to understand the passage from $c<a$ to $c>a$ is to follow the minimum-energy function for the former until its intersection with the latter. Following that reasoning in the setting of Fig. 4 leads to the interpretation that, under intraplanar stress, c at first decreases very slightly from 1.46 to 1.41 a.u. Between $a=3.5$ and 3.4 a.u. the molecular $2L$ becomes a band overlap metal (see Sec. IV). This change in bonding is reflected in the somewhat more rapid increase of c with declining a evident in Fig. 4. Finally, atomic ordering becomes energetically preferably with a discontinuous jump in c/a.

An alternative perspective on the process is given in Fig. 5 which shows E_{tot}/N as a function of c for $a=2.7$ a.u. (near the value for which the molecular and atomic systems have the same optimum total energy per atom). Remarkably, the barrier, which is only about 0.4 mhartree, occupies the whole region $1.9<c<2.5$ a.u. The small ripples in the plateau evident in Fig. 5 are numerical artifacts, as evidenced by the fact that they disappear when the density of quadrature points in the exchange-correlation fitting is increased. Thus we do not find any family of intermediate structures, which would appear in Fig. 5 as local minima in that region. We are unable, therefore, to confirm an ultrathin film analog of the metastable structures (intermediate in density between atomic and molecular ones) predicted by Wigner and Huntington.[1] Neither do we find evidence for the closely related prediction by Brovman, Kagan, and Kholas of a "quadratic" family of nearly degenerate structures related by shifting of ions parallel to the c axis while preserving the projection in a plane perpendicular to that axis.

Next we return to the molecular ordering in the $1L$. Recall from Table II that the differences in total energy among the three genuinely molecularly ordered $1L$'s are quite small, on the order of the estimated precision of the calculation. [Once again we omit $M(G,m)$ as a

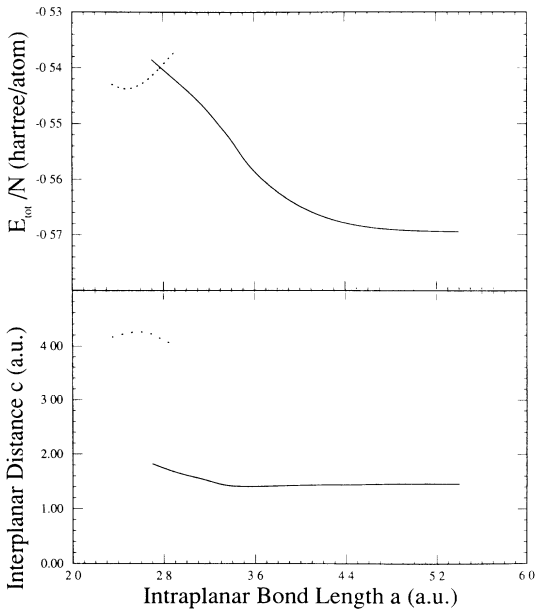

FIG. 4. Optimum E_{tot}/N and c as a function of optimized a for both $D_<(S,\mathrm{Ov})$ (solid curve) and $D_>(S,\mathrm{Ov})$ (dotted curve).

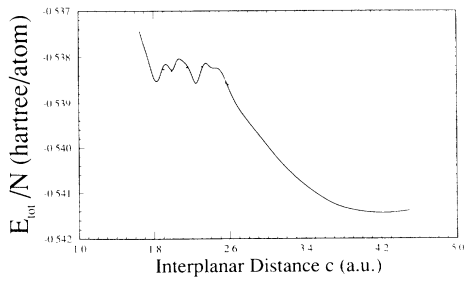

FIG. 5. E_{tot}/N for $D(S,\mathrm{Ov})$ as a function of interplanar distance c for fixed $a=2.7$ a.u. Solid curve: normal mesh for numerical quadrature in exchange-correlation fitting. Dashed curve: high-density mesh.

classificational anomaly.] This is suggestive of a low barrier to in-plane rotation. In contrast, the lattice parameter differences among the three are significant: the binding is quite insensitive to substantial lattice parameter shifts so long as molecular bonding is maintained.

Considered as bundles of molecular chains, only $^{45}M(S,m)$ exhibits both intramolecular and intermolecular spacings along those chains which are moderately close to the values for a periodically bounded linear chain (i.e. ring), namely $s=5.64$ a.u. for l fixed at 1.41 a.u. in the 14-atom case,[23] as compared with 1.45 and 6.5 a.u. for $^{45}M(S,m)$. Of course, $^{0}M(S,m)$ cannot exhibit this behavior because of its intrinsic constraint, $(l+s)=a=b$. The behavior of the $^{0}M(R,m)$ system is less obvious since it appears to be little more than a minutely relaxed version of $^{0}M(S,m)$.

In crystalline H it was suggested long ago[1] that under pressure l and s tend to a common value with the key qualitative issue being whether the process is continuous or involves a discontinuous change of lattice structure. Min, Jansen, and Freeman[6(b)] have studied the question in detail for the case of the $Pa3$ molecular crystal driven toward the sc atomic crystal. In our notation, they found [cf. Sec. IV B and Fig. 8 of Ref. 6(b)] that l was essentially constant at 1.40 a.u. down to a $Pa3$ lattice constant equivalent to $r_s \simeq 1.1$ a.u. (r_s is the familiar Wigner electron-sphere radius). Below that r_s value Ref. 6(b) found that l rises rapidly to the asymptotic value $l=0.5352\ a$ (where a is the $Pa3$ lattice parameter) and follows that relation as far as their calculations went. The asymptotic relationship comes from minimizing the Madelung energy, which should dominate at high compression, for the $Pa3$ structure. It is considerably shorter than the value for which $Pa3$ corresponds to sc, $l=(\sqrt{3}/2)a$.

A $1L$ analog to the crystalline case studied in Ref. 6(b) is the passage from $^{45}M(S,m)$ to the special geometry corresponding to fcc(100). We have treated this with a detailed series of calculations.[24] (Note that this is a constrained calculation; relaxation by molecular rotation out of the plane was not allowed.) The optimal bond length l and $E_{\rm tot}/N$ as a function of the atomic density parameter ρ_s are shown in Fig. 6 for both $^{45}M(S,m)$ and the monatomic simple-square system $M(S,a)$ which corresponds to fcc(100). Here ρ_s is the planar analog to the crystalline r_s. For ν atoms per unit cell $\pi\rho_s^2=$ (cell area)/ν. The most remarkable feature of Fig. 6(b) is that it is nearly indistinguishable qualitatively from Fig. 8 of Min, Jansen, and Freeman.[6(b)] In particular, l stays almost exactly at its equilibrium $1L$ value, $l_{\rm equilib}=1.45$ a.u. until the system is substantially compressed. Between $\rho_s=1.31$ and 1.28 a.u. the system goes metallic (by band overlap; further discussion below) and l dips to a minimum of 1.40 a.u. For $\rho_s<1.28$ a.u. l increases rapidly. (Almost identical behavior occurs for the metallization of the $c<a$ $2L$'s; see Sec. IV.) Note that the monatomic curve in our case must obey $l=a$.

Determination of the atomic density at which the molecular and atomic ordering become indistinguishable is a demanding task, as evident from the two panels of

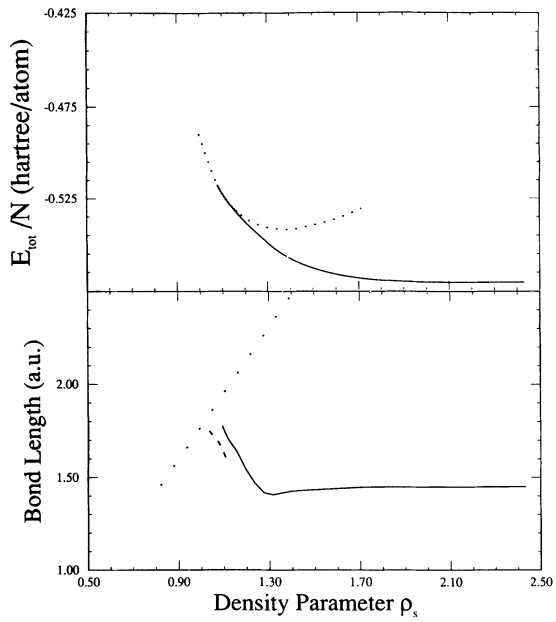

FIG. 6. Transition of the $^{45}M(S,m)$ system to the $M(S,a)$ system as monitored by the optimized total-energy per atom (upper panel) and the intramolecular bond length l (lower panel), both as a function of the planar density parameter ρ_s. [For ν atoms per unit cell $\pi\rho_s^2=$ (cell area)/ν.] Dotted curve represents atomic system. Solid curve represents molecular system *including* bond-aligned p-type fitting function. Dashed curve (lower panel only) represents molecular system *excluding* bond-aligned p-type fitting function.

Fig. 6. The upper panel shows the smooth, featureless fashion in which the two total-energy curves join. The lower panel shows l for both $^{45}M(S,m)$ and $M(S,a)$ (for which $l=a$, of course). Included in that lower panel is a cautionary note. Usage (solid curve) or omission (dashed curve) of a true p-type fitting function which is centered on each atom of a molecular pair and aligned along the molecular axis makes a discernible shift in the position of the molecular-system curve. The shift illustrates the difficulty in obtaining a precise value for l when high atomic density is combined with a situation of rapidly changing bonding. Our best estimate of the point of merger is $\rho_s=1.05\pm0.05$ a.u. (simple-square lattice parameter of 1.86 a.u.). This is remarkably close to the r_s value predicted by Min, Jansen, and Freeman[6(b)] to be the point at which the crystal goes over to Madelung behavior (and hence does not achieve the sc structure). Within numerical precision, our calculation does not show an analogous Madelung structure as preferred over fcc(100).

The bond-length dip near $\rho_s=1.30$ a.u. may perhaps be rationalized as arising from the changing admixture of the normal $^{1}\Sigma_g^{+}$ molecular bonding state with the repulsion from $^{3}\Sigma_u^{+}$ state [minimum at 7.85 a.u. (Ref. 25)] from the next-nearest H atom along the diagonal. With continued compression (sufficiently small ρ_s), metallic bonding begins to dominate and l begins its increase toward the value corresponding to atomic spacing.

IV. ONE-ELECTRON PROPERTIES

The risks associated with interpreting Kohn-Sham eigenvalues as one-electron energies are well known[26] and should be borne in mind throughout this discussion. Two simple, relevant band parameters (Fermi energy or gap plus occupied bandwidth) are given in Table V for all 22 systems. Energy bands for an exemplary molecular $2L$, $D_<(S,\mathrm{Ov})$, the corresponding atomic $2L$, $D_>(S,\mathrm{Ov})$, and both the low-aspect and high-aspect $3L$'s, $T_<(S,\mathrm{Ov})$ and $T_>(S,\mathrm{Ov})$ are plotted in Fig. 7.

With an odd number of electrons per unit cell, the atomiclike $1L$'s and all the $3L$'s are metallic by construction. As we have already seen, the $2L$'s with $c>a$ are essentially weakly perturbed pairs of $1L$'s; unsurprisingly, they too are metallic. As would be expected, all the metallic nL's have much greater occupied bandwidth W than all the insulators. W for the hexagonal systems is typically 0.1–0.7 eV larger than for the corresponding (in the sense of stacking) square nL's, consistent with the ordering of their cohesive energies.

A striking feature of the results in Table V is the clear dominance of the molecular ordering mechanism in determining these key quantities, as shown by the number of pairs of systems each with essentially the same band parameters. The common feature of each pair is whether or not there is H dimerization. This overwhelms such differences as stacking or lattice symmetry.

As isovalent systems of the same symmetry, the monatomic Li and H $1L$'s would be expected to have very similar work functions ($-\varepsilon_F$), and the same could be expected for $D_>(H,\mathrm{Ov})$, $D_>(H,\mathrm{Op})$, $D_>(S,\mathrm{Ov})$, and $D_>(S,\mathrm{Op})$, the $2L$ metals. The actual comparison with hexagonal Li $1L$'s and open hexagonal $2L$'s (Ref. 27) confirms the point: $\varepsilon_F(\mathrm{Li},H,1L)=-3.5$ eV, $\varepsilon_F[M(H,a)]=-3.3$ eV, $\varepsilon_F(Li,H,2L)=-3.6$ eV, $\varepsilon_F[D_>(H,\mathrm{Ov})]=-3.8$ eV, and $\varepsilon_F[D_>(H,\mathrm{Op})]=-3.7$ eV.

The most interesting aspect of the electronic structure is the overlap metallization transition in the filamentary systems. Again, two cases are considered. For $D_<(S,\mathrm{Ov})$, Fig. 8(a) shows that metallization occurs by indirect gap closure between the Γ and K points. Both the rate of closure and the interval separating bands at a given point in the BZ are roughly constant over a strikingly large range of a values. We estimate metallization to occur at about $a=3.45$ a.u., $c=l=1.42$ a.u. As ${}^{45}M(S,m)$ changes to $M(S,a)$ metallization is also by indirect gap closure between J and K [see Fig. 8(b)] with

TABLE V. Calculated energy-band parameters $\varepsilon_{\mathrm{gap}}$ or ε_f, as appropriate, and W (the occupied bandwidth) for H $1L$, $2L$, and $3L$'s in the indicated structures at their calculated equilibrium lattice constants. All values are in eV.

System	$\varepsilon_{\mathrm{gap}}$	ε_F	W
${}^0M(R,m)$	6.8		3.1
${}^0M(S,m)$	6.9		2.7
${}^{45}M(S,m)$	9.1		2.1
$M(G,m)$	0 (semimetal)	−3.2	8.2
$M(R,a)$		−4.3	9.9
$M(H,a)$		−3.3	14.0
$M(S,a)$		−3.7	13.5
${}^0D(R,B)$	6.1		3.4
${}^0D(R,\mathrm{Ov})$	6.1		3.5
$D_<(H,\mathrm{Ov})$	8.5		2.2
$D_<(S,\mathrm{Ov})$	8.6		2.1
$D_<(H,\mathrm{Op})$	see $M(G,a)$		
$D_>(H,\mathrm{Ov})$		−3.8	14.6
$D_>(H,\mathrm{Op})$		−3.7	14.7
$D_>(S,\mathrm{Ov})$		−4.2	14.2
$D_>(S,\mathrm{Op})$		−4.3	14.2
$T_<(H,\mathrm{Ov})$		−4.9	12.5
$T_<(S,\mathrm{Ov})$		−5.1	11.8
$T_>(H,\mathrm{Ov})$		−3.9	15.0
$T_>(H,E)$		−3.9	15.1
$T_>(S,\mathrm{Ov})$		−4.3	14.7
$T_>(S,E)$		−4.3	14.6

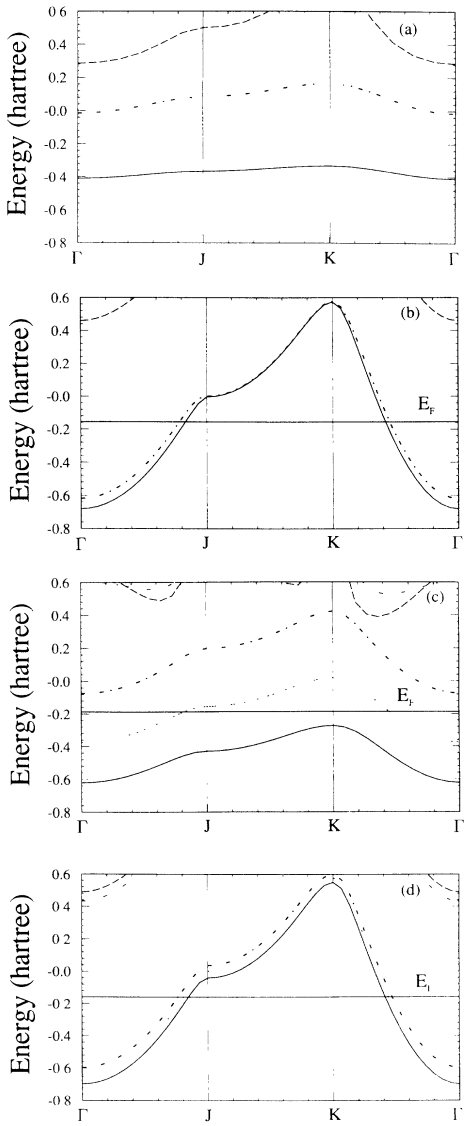

FIG. 7. Energy bands for square H $2L$'s and $3L$'s (a) $D_<(S,\mathrm{Ov})$; (b) $D_>(S,\mathrm{Ov})$; (c) $T_<(S,\mathrm{Ov})$; (d) $T_>(S,\mathrm{Ov})$.

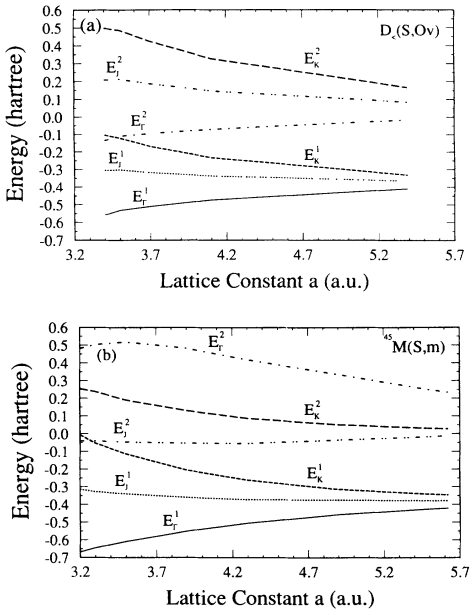

FIG. 8. Indirect gap closure in filamentary systems under applied stress. Energies are in hartree (a) $D_<(S,\mathrm{Ov})$; (b) $^{45}M(S,m)$.

$a=3.22$ a.u. and $l=1.41$ a.u. the estimated lattice parameters at zero gap. These values of l at metallization are quite comparable with the crystalline prediction of 1.40 a.u. by Min, Jansen, and Freeman.[6(b)]

V. COMMENTS

H n layers with $n=1,2,3$ are dominated by molecular bonding with metallization by band overlap, much as in crystalline systems. The structural energetics of the systems studied suggest strongly that filamentary structures rather than some crystalline-symmetry expitaxy will dominate the growth of H slabs.

Akin to most other crystalline and film LDA total-energy calculations, this study relied on a simple calculational strategy, namely an exhaustive search, with respect to the lattice parameters, of a small, finite set of structures (22 here). At $n=3$ a well-known difficulty in this strategy was encountered. None of the structures treated is bound with respect to separation into three $1L$'s or a $1L$ plus a $2L$. The challenge is not the lack of candidate structures. We have remarked on the likelihood of a rectangular $3L$ as energetically favored. Rather, the challenge is the rapid growth, with increasing n, of candidate structures. The number of $2L$'s and $3L$'s one can identify from the $Pa3$ molecular-crystal structure is only one example. A real barrier to progress is the absence of any obvious qualitative or semiquantitative procedure to identify high-priority candidate structures (other than the obvious rectangular one) which are likely to produce a bound $3L$. Contemporary molecular calculations address the problem by inclusion of energy-minimization methods within the computation itself (instead of by some screening or estimation technique). To our knowledge this has not been done for crystalline or film calculations (except by stochastic methods,[28] which are not at issue here). Although certainly it would be of value to incorporate such techniques, a predictive screening procedure prior to computation would be helpful both for physical insight and for reduction of computational effort.

ACKNOWLEDGMENTS

We thank Professor J.-L. Calais and Professor H. J. Monkhorst for several helpful conversations and for alerting us to various references. J.Z.W. thanks Professor Bill Meath for a helpful conversation. J.Z.W., J.R.S., and S.B.T. were supported in part by the U.S. Army Research Office under Contract No. DAA L03-87-0046. J.C.B. was supported by the U.S. Department of Energy. This paper was completed while S.B.T. was at the Center for Materials Science of Los Alamos National Laboratory, for which opportunity he thanks D. Parkin and A. M. Boring.

[1]E. Wigner and H. B. Huntington, J. Chem. Phys. **3**, 764 (1935).
[2]N. W. Ashcroft, Phys. Rev. Lett. **21**, 1748 (1968).
[3]E. G. Brovman, Yu. Kagan, and A. Kholas, Zh. Eksp. Teor. Fiz. **61**, 2429 (1971); **62**, 1492 (1972) [Sov. Phys. JETP **34**, 1300 (1972); **35**, 783 (1972)].
[4]D. E. Ramaker, L. Kumar, and F. E. Harris, Phys. Rev. Lett. **34**, 812 (1975).
[5]S. Chakravarty, J. H. Rose, D. Wood, and N. W. Ashcroft, Phys. Rev. B **24**, 1624 (1981).
[6](a) B. I. Min, H. J. F. Jansen, and A. J. Freeman, Phys. Rev. B **30**, 5076, (1984); (b) **33**, 6383 (1986).
[7](a) T. W. Barbee III, A. Garcia, M. L. Cohen, and J. L. Martins, Phys. Rev. Lett. **62**, 1150 (1989); (b) T. W. Barbee, A. Garcia, and M. L. Cohen, Nature **340**, 369 (1989).
[8]N. F. Mott, Proc. Phys. Soc. London **62**, 416 (1949).
[9]L. F. Mattheiss, Phys. Rev. **123**, 1209 (1961).
[10]D. H. Liskow, J. M. McKelvey, C. F. Bender, and H. F. Schaefer, Phys. Rev. Lett. **32**, 933, 1331(E) (1974).
[11]M. Kertesz, J. Koller, and A. Azman, Theor. Chim. Acta **41**, 89 (1976).
[12]F. E. Harris, and J. Delhalle, Phys. Rev. Lett. **39**, 1340 (1977).
[13]J.-M. Andre, J.-L. Bredas, J. DelHalle, Y. Kalenov, L. Piela, and J. L. Calais, Int. J. Quantum Chem. S **14**, 419 (1980).
[14]M. Seel, P. S. Bagus, and J. Ladik, J. Chem. Phys. **77**, 3123 (1982).
[15]J. C. Boettger and S. B. Trickey, J. Phys. Condens. Matter **1**, 4323 (1989); Phys. Rev. **32**, 1356 (1985); S. B. Trickey, G. H. F. Diercksen, and F. Müller-Plathe, Astrophys. J. **336**, L37, (1989); J. Z. Wu, S. B. Trickey, and J. C. Boettger, Phys. Rev. B **42**, 1663, (1990); **42**, 1668 (1990), and references cited therein.
[16]J. Z. Wu, J. R. Sabin, S. B. Trickey, and J. C. Boettger, Int. J. Quantum Chem. S **24**, 873 (1990).
[17]J. Z. Wu, D. E. Meltzer, J. R. Sabin, S. B. Trickey, and J. C.

Boettger (unpublished).
[18]J. W. Mintmire, J. R. Sabin, and S. B. Trickey, Phys. Rev. B **26**, 1743 (1982).
[19]F. B. van Duijneveldt, IBM Report RJ945 (1971) (unpublished).
[20]T. Terzibaschian and R. Enderlein, Phys. Status Solidi B **133**, 443 (1986).
[21]*Tables of Interatomic Distances and Configurations in Molecules and Ions—Supplement 1956-9* (The Chemical Society, London, 1965).
[22]P. Siegbahn and B. Liu, J. Chem. Phys. **68**, 2456 (1978).
[23]This value is obtained from Ref. 14 by computing distance along the periodic arc; those authors give the chord length as the intermolecular separation.
[24]The technically interested reader is cautioned that although this is a $1L$ system with at most two electrons per unit cell, determination of the point at which ${}^{45}M(S,m)$ has gone over to fcc(100) is an extremely demanding calculation. Extensive testing, beyond that discussed in the text, of BZ meshes, numerical integral mesh densities, and fitting function basis sets was needed in order to achieve the required stability and precision.
[25]W. Kolos and L. Wolniewicz, J. Chem. Phys. **43**, 2429 (1965).
[26]*Density Functional Theory of Many-Fermion Systems*, edited by S. B. Trickey, Advanced Quantum Chemistry Vol. 21 (Academic, San Diego, 1990).
[27]J. C. Boettger, S. B. Trickey, F. Müller-Plathe, and G. H. F. Diercksen, J. Phys. Condens. Matter **2**, 9589 (1990).
[28]R. Car and M. Parrinello, Phys. Rev. Lett. **55**, 2471 (1985).